Jambura Journal of Biomathematics

RESEARCH ARTICLE

Hemodynamic Modeling of Branch Retinal Artery Occlusion Involving Asymmetric Vascular Stenosis

Basuki Widodo[1,✉], **Ni Putu Anna Ristia Dewi**[1], **Yuni Keputri Muarifadila**[1], **Annisa Dwi Sulistyaningtyasa**[1], **Arif Fatahillah**[2], **Tri Rahayuningsih**[3]

[1]Department of Mathematics, Sepuluh Nopember Institute of Technology, Surabaya, Indonesia

[2]Department of Mathematics Education, University of Jember, Jember, Indonesia

[3]Department of Agroindustry Technology, University of Wijaya Kusuma Surabaya, Surabaya, Indonesia

✉Corresponding author. Email: *b.widodo@its.ac.id*

Article Identity
Jambura J. Biomath.
Volume 7 Issue 1 Pages 197 – 210
March 2026, E-ISSN 2723-0317

Article History
Received 24 November 2025
Revised 4 March 2026
Accepted 30 March 2026
Published 30 March 2026

Keywords
Hemodynamic, Stenosis, BRAO, Navier–stokes, FVM, SIMPLE algorithm

Editorial office: Department of Mathematics, Universitas Negeri Gorontalo, Jln. Prof. Dr. Ing. B. J. Habibie, Bone Bolango 96554, Indonesia

To Cite this Article: Widodo B et al.. Hemodynamic Modeling of Branch Retinal Artery Occlusion Involving Asymmetric Vascular Stenosis. Jambura Journal of Biomathematics. 2026;7(1):197-210. doi:10.37905/jjbm.v7i1.26

Abstract. *The narrowing of retinal blood vessels, especially in conditions involving branch retinal artery occlusion (BRAO), can cause gradual and painless vision deterioration. Such vascular obstruction is also a contributing factor to eye stroke. This study investigates the influence of three asymmetric stenosis geometries, namely Bell–Cosine, Cosine–Overlapping, and Bell–Overlapping, on fluid flow characterized as Newtonian, incompressible, and steady. The mathematical formulation is derived from the Navier–Stokes equations, discretized using the Finite Volume Method (FVM) and solved through the Semi-Implicit Method for Pressure-Linked Equations (SIMPLE) algorithm. Numerical simulations are performed in MATLAB with variations in stenosis length. The results demonstrate how different geometric shapes and stenosis lengths affect blood flow rate and pressure distribution. Among all configurations, the Bell–Cosine geometry consistently produces a flow rate above the normal threshold and a pressure level below the normal range for each stenosis length ($40\,\mu m$, $50\,\mu m$, $60\,\mu m$, $70\,\mu m$), compared with the other geometries. For every geometric arrangement, stenosis length plays a role in altering the flow behavior and pressure field around the constriction, while the peak velocity and peak pressure remain essentially unchanged.*

1. Introduction

Mathematics is a foundational discipline that significantly contributes to societal development by providing tools to understand various objects, phenomena, and underlying mechanisms within specific fields [1]. One important branch of applied mathematics is Computational Fluid Dynamics (CFD), which focuses on analyzing systems involving fluid motion. This approach is widely used to simulate numerous physical processes, including the flow of blood through arteries and veins [2–4]. Among the medical conditions related to arterial circulation is ocular stroke, a disorder characterized by blockage within the retinal vasculature [5, 6]. One form of retinal arterial stenosis frequently encountered is Branch Retinal Artery Occlusion (BRAO). BRAO refers to an obstruction occurring in the smaller branches of the retinal arteries, most commonly in the temporal region. This blockage

typically arises from emboli, vasculitis, coagulation abnormalities, migraine-induced vasospasms, or inflammatory responses. Of these, embolic obstruction is the predominant cause, with emboli often originating from cholesterol deposits, calcium fragments, or platelet aggregates. BRAO may also develop as a result of retinal vessel dilation (macroaneurysm), which can trigger turbulent flow leading to occlusion, as well as inflammation and vasospasm. Several risk factors increase susceptibility to this condition, including hypertension, carotid occlusive disease or atherosclerosis, coronary heart disease, and elevated cholesterol levels [7]. Previous research indicates that many patients can still retain relatively good vision by undergoing appropriate medical evaluation [8]. In cases of BRAO caused by macroaneurysm, combined anti-VEGF therapy and focal laser treatment have been shown to produce substantial improvement in visual outcomes [8, 9].

A number of researchers have explored the issue of vascular occlusion. Kumar and Kumar (2023) investigated various stenosis geometries in blood vessels and demonstrated that arterial wall shape, magnetic field effects, and the Darcy number significantly influence blood flow velocity, particularly in bell-shaped stenoses [10]. Meanwhile, the study by Fatahillah, Widodo, and Roslan (2025) analyzed Branch Retinal Artery Occlusion and found that a stenosis thickness of 90% poses severe risk because both blood flow velocity and pressure exceed normal physiological ranges [4, 9, 11]. In this simulation, blood is considered a Newtonian fluid with incompressible and steady properties.

Recent contributions published in the *Jambura Journal of Biomathematics* also illustrate the breadth of mathematical approaches currently being applied to biomedical problems. Aruchamy et al. converted Doppler-based fetal heart blood-flow information into an intuitionistic fuzzy total edge magic labelling framework to interpret fetal heart rate patterns, whereas Das et al. formulated a fractional-order leukemia model and investigated its qualitative properties through stability analysis and numerical simulation [12, 13]. Although these studies address different biomedical systems, they demonstrate that physiological interpretation, mathematical structure, and computational analysis can be integrated effectively within a biomathematical setting. This perspective is relevant to the present BRAO study, where clinically meaningful retinal hemodynamics are likewise examined through mathematical modeling and numerical computation.

Despite these advances, previous hemodynamic studies have primarily focused on isolated stenosis shapes, symmetric constrictions, or single-geometry analyses, leaving the comparative behavior of compound asymmetric stenosis configurations in Branch Retinal Artery Occlusion (BRAO) insufficiently understood. In particular, the influence of stenosis length has rarely been investigated as an independent geometric parameter under identical retinal hemodynamic conditions.

Therefore, this study introduces several contributions. First, it provides a comparative hemodynamic analysis of three asymmetric composite stenosis geometries—Bell–Cosine, Bell–Overlapping, and Cosine–Overlapping—specifically in the context of BRAO. Second, the study systematically examines the influence of geometric variations, including differences in stenosis thickness (severity) and normalized stenosis length along the arterial segment. Third, the research analyzes how these geometric variations affect not only the magnitude but also the spatial distribution of velocity and pressure fields within the retinal artery. Finally, the proposed mathematical model is implemented using a MATLAB-based finite volume framework and validated through ANSYS FLUENT simulations, providing cross-platform numerical verification that enhances the robustness and reliability of the predicted hemodynamic behavior. This study is the first to compare three asymmetric stenosis geometries (Bell–Cosine, Bell–Overlapping, and Cosine–Overlapping) under identical BRAO conditions and to systematically analyze the influence of stenosis length on the spatial distribution of velocity and pressure. Furthermore, the combined MATLAB–ANSYS workflow serves as a two-stage verification mechanism, further strengthening the reliability of the numerical results.

2. Mathematical Formulation

The mathematical model used in this problem is the continuity equation and the momentum equation:

$$\frac{\partial u_i}{\partial x} = 0,$$
$$\frac{\partial u_i}{\partial t} + \frac{\partial (u_i u_j)}{\partial x} = -\frac{1}{\rho}\nabla P + \mu \frac{\partial u_i}{\partial x}.$$

The depiction of the problem regarding variations in stenosis geometry can be represented in the following Figure 1 [10].

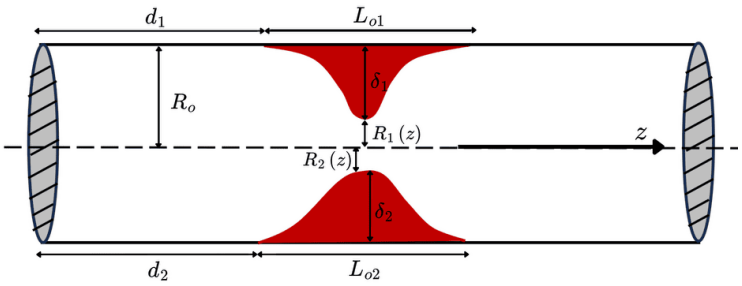

Figure 1. Asymmetric Bell–Cosine Shaped Stenosis.

Model equations for asymmetric Bell–Cosine shaped geometry:

$$R_{1,2}(z) = \begin{cases} R_0 - \delta_s \exp\left[-\dfrac{m^2}{R_0^2}\left(z - d_1 - \dfrac{L_{o1}}{2}\right)^2\right], & d_1 \le z \le d_1 + L_{o1}, \\ R_0 - \dfrac{\delta_s}{2}\left(1 + \cos\left[\dfrac{2\pi}{L_{o2}}\left(z - d_2 - \dfrac{L_{o2}}{2}\right)\right]\right), & d_2 \le z \le d_2 + L_{o2}, \\ R_0, & \text{otherwise.} \end{cases}$$

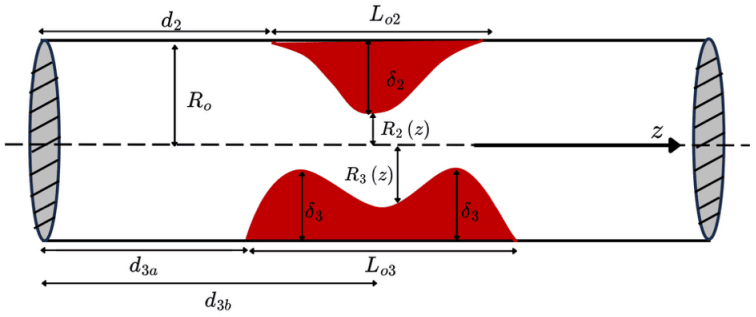

Figure 2. Asymmetric Cosine–Overlapping Shaped Stenosis.

Model equations for asymmetric Cosine–Overlapping shaped geometry:

$$R_{2,3}(z) = \begin{cases} R_0 - \dfrac{\delta_s}{2}\left(1 + \cos\left[\dfrac{2\pi}{L_{o2}}\left(z - d_2 - \dfrac{L_{o2}}{2}\right)\right]\right), & d_2 \le z \le d_2 + L_{o2}, \\ R_0 - [r_a - r_b], & \text{in the overlapping region,} \\ R_0, & \text{otherwise,} \end{cases}$$

with

$$r_a = \begin{cases} \dfrac{\delta_s}{2}\left(1+\cos\dfrac{2\pi(z-d_{3a})}{L_{o3}}\right), & d_{3a} \le z \le d_{3b}, \\ 0, & \text{otherwise}, \end{cases}$$

$$r_b = \begin{cases} \dfrac{\delta_s}{2}\left(1+\cos\dfrac{2\pi(z-d_{3b})}{L_{o3}}\right), & d_{3b} \le z \le d_{3a}+L_{o3}, \\ 0, & \text{otherwise}. \end{cases}$$

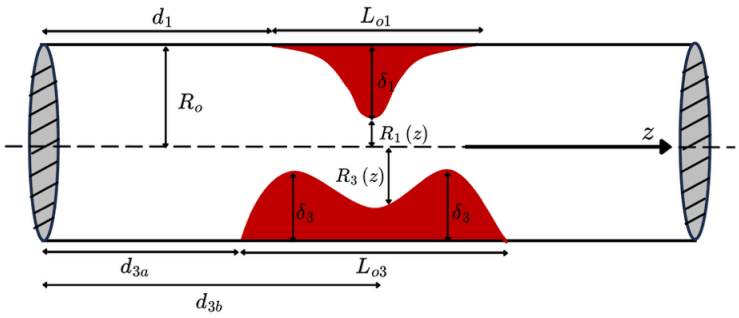

Figure 3. Asymmetric Bell–Overlapping Shaped Stenosis.

Model equations for asymmetric Bell–Overlapping shaped geometry:

$$R_{1,3}(z) = \begin{cases} R_0 - \delta_s \exp\left[-\dfrac{m^2}{R_0^2}\left(z-d_1-\dfrac{L_{o1}}{2}\right)^2\right], & d_1 \le z \le d_1+L_{o1}, \\ R_0-[r_a-r_b], & \text{in the overlapping region}, \\ R_0, & \text{otherwise}. \end{cases}$$

with

$$r_a = \begin{cases} \dfrac{\delta_s}{2}\left(1+\cos\dfrac{2\pi(z-d_{3a})}{L_{o3}}\right), & d_{3a} \le z \le d_{3b}, \\ 0, & \text{otherwise}, \end{cases}$$

$$r_b = \begin{cases} \dfrac{\delta_s}{2}\left(1+\cos\dfrac{2\pi(z-d_{3b})}{L_{o3}}\right), & d_{3b} \le z \le d_{3a}+L_{o3}, \\ 0, & \text{otherwise}, \end{cases}$$

where:

$R_1(z)$ = radius of the artery with Bell-shaped stenosis,
$R_2(z)$ = radius of the artery with Cosine-shaped stenosis,
$R_3(z)$ = radius of the artery with Overlapping-shaped stenosis,
R_0 = radius of the normal artery,
δ_{s1} = peak height of the Bell-shaped stenosis,
δ_{s2} = peak height of the Cosine-shaped stenosis,
δ_{s3} = peak height of the Overlapping-shaped stenosis,
L_{o1} = total length of the Bell-shaped stenosis,
L_{o2} = total length of the Cosine-shaped stenosis,

L_{o3} = total length of the Overlapping-shaped stenosis,
d_1 = location of the Bell-shaped stenosis,
d_2 = location of the Cosine-shaped stenosis,
d_{3a} = location of the first curve of the Overlapping-shaped stenosis,
d_{3b} = location of the second curve of the Overlapping-shaped stenosis,
z = flow direction,
L = artery length,
m = constant parameter.

The boundary conditions are:

$$u(z,t) = 0, \quad v(z,t) = 0, \quad \frac{\partial u}{\partial z}(z,t) = 0 \quad \text{at} \quad R = 0,$$
$$u(z,t) = \frac{\partial R}{\partial t}, \quad w(r,z,t) = 0 \quad \text{at} \quad R = R(z,t).$$

The study provides the inlet velocity value at $x = 0$, as shown in the following equation in [9]:

$$u = 2U_0 \left(1 - \left(\frac{r}{R(z)}\right)^2\right).$$

3. Methods

The initial stage of this research involves formulating the mathematical model that will serve as the basis for simulation and analysis. The model is constructed from the Navier–Stokes equations, which govern fluid motion, and is modified to reflect the properties of the blood flow and the specific stenosis geometries under investigation. The stenosis configurations examined in this study consist of the Asymmetric Bell–Cosine, Cosine–Overlapping, and Bell–Overlapping shapes. Once the model is defined, it is discretized using the Finite Volume Method (FVM), a numerical technique that partitions the computational domain into a series of control volumes, each enclosed by control surfaces [14–16]. After discretization, the governing equations are solved using the SIMPLE (Semi-Implicit Method for Pressure-Linked Equations) algorithm, which applies a predictor–corrector approach for pressure calculation on a staggered grid system. This procedure is typically illustrated through steady, laminar, two-dimensional flow in Cartesian coordinates [2, 17, 18]. This workflow is consistent with recent JJBM studies that combine formal mathematical models with qualitative analysis or computational procedures to interpret biomedical phenomena [12, 13].

Although retinal arteries are relatively small (200–300 μm in diameter), several studies have shown that the Newtonian fluid assumption remains reasonable when the vessel diameter exceeds 150 μm, since the shear rate is sufficiently high to reduce non-Newtonian effects [4, 15]. Therefore, the Newtonian model is considered appropriate for BRAO simulations and has also been adopted in similar CFD studies.

MATLAB was initially used to perform preliminary two-dimensional finite volume method (FVM) simulations to evaluate the effect of stenosis length. These initial simulations served as a verification step before proceeding to a more comprehensive three-dimensional analysis. Subsequently, the refined 3D geometry was constructed and meshed in ANSYS Workbench, followed by the specification of boundary conditions in ANSYS FLUENT. The 3D simulations were then carried out in ANSYS FLUENT to capture more detailed flow features, including recirculation zones and pressure distribution. Finally, the results obtained from MATLAB and ANSYS FLUENT were compared, validated, and interpreted to support the final conclusions of the study [19, 20].

4. Results and Discussion

From the literature review, several parameters influencing blood flow rate and pressure distribution in the presence of stenosis within the retinal artery were identified [21–23]. The first stage of the analysis involved conducting simulations to evaluate how variations in stenosis length affect blood flow rate across all geometric configurations, namely Bell–Cosine, Bell–Overlapping, and Cosine–Overlapping, using MATLAB. These simulations were performed with an initial inlet velocity of 0.3 m/s and stenosis length variations of $40\,\mu$m, $50\,\mu$m, $60\,\mu$m, and $70\,\mu$m.

Table 1. Values of parameters for blood flow rate in BRAO.

Parameters	Values
Retinal artery diameter	$265 \pm 20\,\mu$m
Blood density	$1.054 - 1.060\ \frac{\text{kg}}{\text{m}^3}$
Viscosity	$0.003\ \frac{\text{kg}}{\text{ms}}$
Hypertensive blood pressure	Systolic: >140 mmHg; Diastolic: >90 mmHg
Velocity artery	$0.19 - 0.49\ \frac{\text{m}}{\text{s}}$
Initial velocity	$0.3\ \frac{\text{m}}{\text{s}}$
Pressure	17331 Pa
Thermal conductivity	$0.44\ \frac{\text{W}}{\text{mK}}$

Based on the simulation results presented in Figure 4, the Bell–Cosine geometry consistently produces a maximum velocity of approximately $1.49\ \frac{\text{m}}{\text{s}}$ for all stenosis length variations, as shown by the dark red regions in the plot. This confirms that the peak velocity remains essentially unchanged regardless of the stenosis length. The overall velocity profile displays a bell-shaped pattern, characterized by smooth increases and decreases around the center of the stenosis. As the stenosis length becomes longer, the region corresponding to higher velocities gradually expands, indicating that although the peak velocity value remains nearly constant, its spatial distribution broadens with increasing stenosis length.

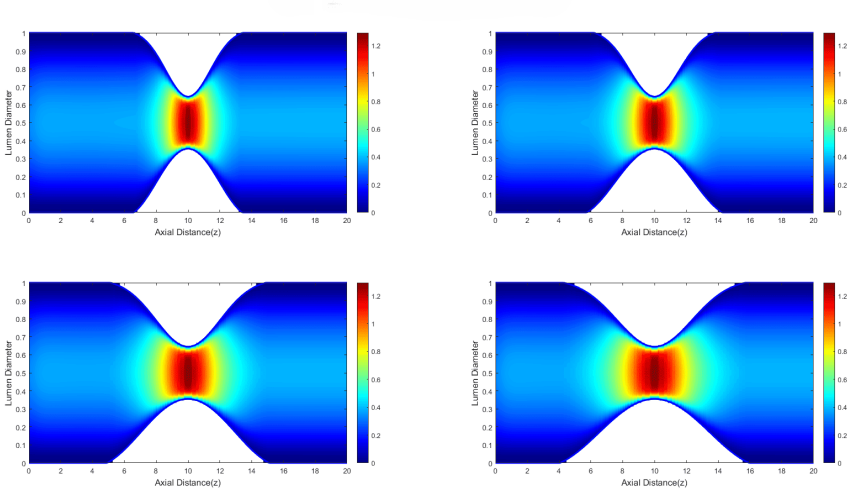

Figure 4. Velocity for Bell–Cosine geometry.

In addition, Figure 5 illustrates that the Bell–Overlapping geometry produces a maximum velocity of approximately $0.94\ \frac{\text{m}}{\text{s}}$ at the center of the domain for all stenosis length variations. This

value remains unchanged for stenosis lengths of $40\,\mu$m, $50\,\mu$m, $60\,\mu$m, and $70\,\mu$m, suggesting that the peak velocity for this geometry is largely unaffected by changes in stenosis length. The velocity profile displays a symmetric bell-shaped pattern, indicating a relatively uniform flow behavior around the stenotic region. As the stenosis length increases, the axial velocity distribution becomes broader, even though the magnitude of the peak velocity itself does not rise.

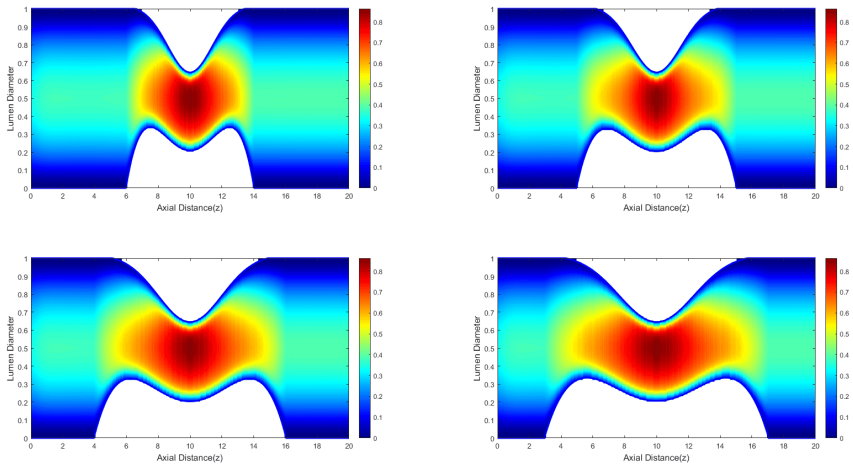

Figure 5. Velocity for Bell–Overlapping geometry.

Figure 6 displays the simulation results for the Cosine–Overlapping geometry, which produces a maximum velocity of about 0.94 $\frac{\text{m}}{\text{s}}$. As observed in the Bell–Overlapping configuration, the peak velocity for the Cosine–Overlapping shape remains fairly constant across all variations in stenosis length. The resulting velocity profile takes on a more elliptical form, characterized by smooth transitions on both sides of the peak region. As the stenosis length increases, this elliptical pattern becomes wider and more distinct, indicating an expansion of the high-velocity region within the flow field.

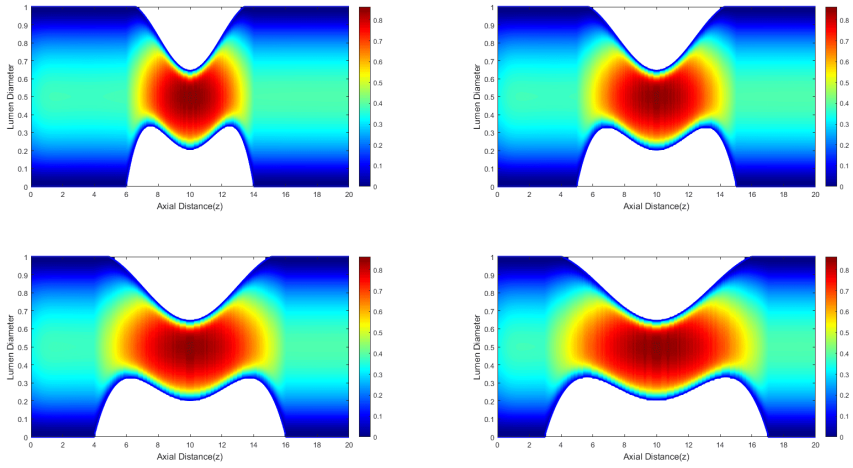

Figure 6. Velocity for Cosine–Overlapping geometry.

From the simulations conducted on all three stenosis geometries across multiple length variations, it is evident that the Bell–Cosine configuration consistently generates the highest peak velocity among the models examined. Its maximum velocity reaches approximately 1.49 $\frac{\text{m}}{\text{s}}$, which is con-

siderably higher than the roughly 0.94 $\frac{\text{m}}{\text{s}}$ peak observed in both the Bell–Overlapping and Cosine–Overlapping geometries. This suggests that the geometric shape of the stenosis has a stronger impact on flow behavior than the stenosis length alone. The sharper and more concentrated narrowing characteristic of the Bell–Cosine shape likely leads to greater fluid acceleration through the constricted region. Furthermore, although variations in stenosis length do not substantially alter the peak velocity across the three geometries, they do influence the extent of the high-velocity zone, causing it to widen as the stenosis becomes longer. In addition, the predicted velocity range $\left(0.19 - 0.49 \frac{\text{m}}{\text{s}}\right)$ is consistent with physiological ranges reported in Goldenberg et al. [22] and Ding et al. [23], indicating that the model is aligned with clinically observed hemodynamic conditions. From a clinical perspective, the widening of disturbed flow regions associated with longer stenosis lengths may correspond to a broader area of impaired perfusion in the retinal artery, potentially increasing the risk of localized ischemic effects. In addition, the high-velocity jets generated in the Bell–Cosine geometry may elevate wall shear stress near the stenotic throat, which could contribute to endothelial stress and may increase the risk of thrombus formation in Branch Retinal Artery Occlusion (BRAO).

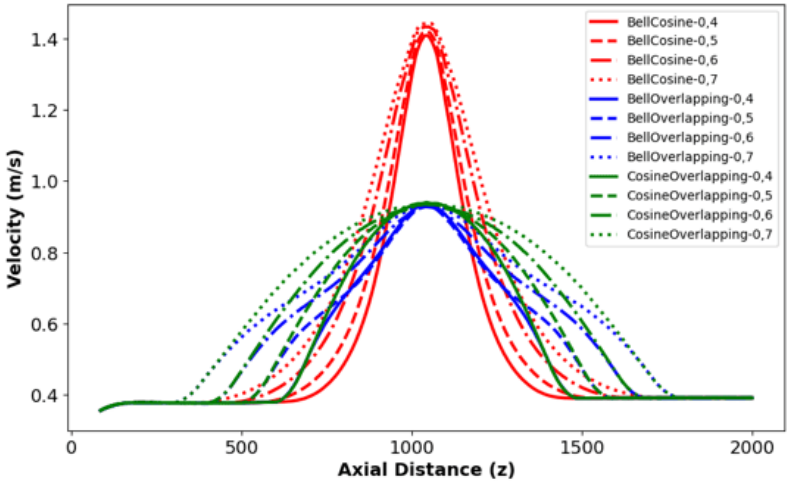

Figure 7. Velocity Profile for Different Stenosis Lengths Across All Geometric Shapes.

Next, based on the simulation results shown in Figure 7, the Bell–Cosine geometry exhibits a minimum pressure of approximately 17,292 Pa across all four stenosis length variations. The pressure profile forms an inverted bell-shaped curve, indicating that as the stenosis length increases, the low-pressure region becomes wider. This means that although the minimum pressure value remains nearly constant, the area experiencing the lowest pressure expands with increasing stenosis length.

Furthermore, Figure 8 illustrates that the Bell–Overlapping geometry yields a minimum pressure of approximately 17,306 Pa for all stenosis length variations, as shown by the dark blue regions in the MATLAB simulation output. The pressure profile forms an inverted bell-shaped curve with a slight indentation near the minimum point, which gradually expands as the stenosis length increases. This indicates that while the minimum pressure value remains unchanged, increasing the stenosis length only broadens the region where the lowest pressure occurs.

Next, Figure 9 shows MATLAB simulation results indicating that the region with the lowest pressure (represented by the dark blue area) expands as the stenosis length increases. From the graph, it is evident that variations in stenosis length do not significantly influence the maximum pressure of the fluid flow. This observation is consistent with the MATLAB output, where the pressure profile shifts outward as the stenosis length becomes longer.

Based on the pressure simulations for all three geometries across the four stenosis length variations, it can be concluded that the Bell–Cosine geometry produces the lowest minimum pressure

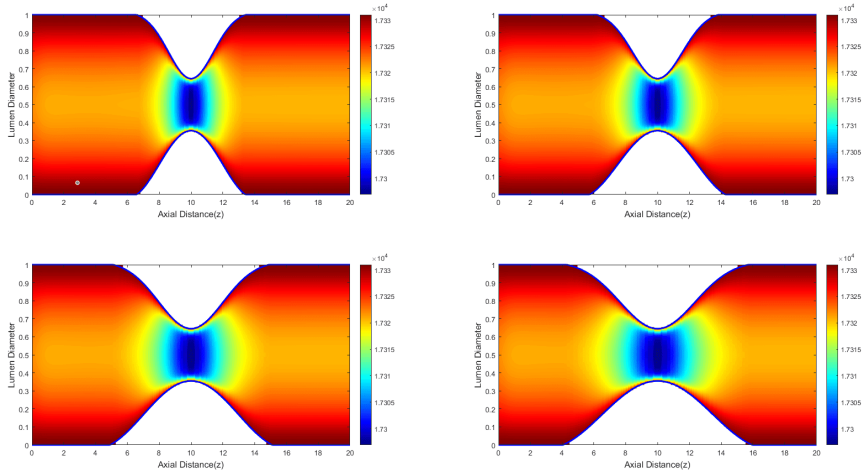

Figure 8. Pressure Distribution Generated by MATLAB for Bell–Cosine Geometry.

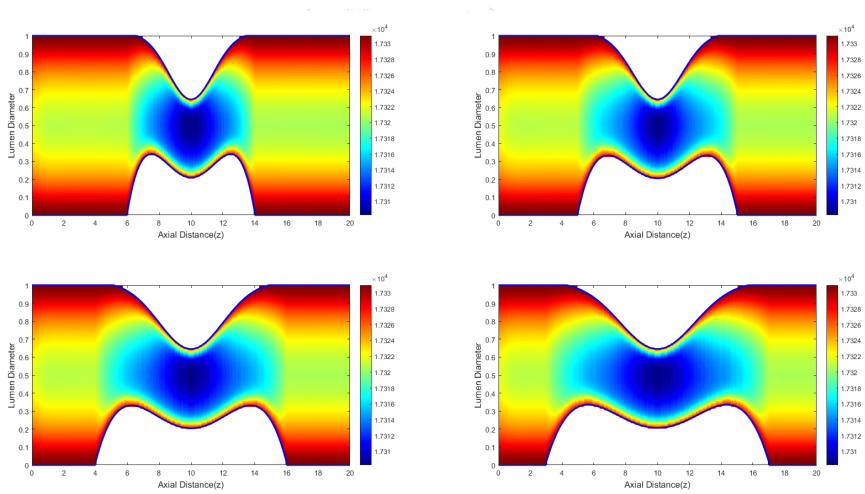

Figure 9. MATLAB Numerical Pressure Output for the Bell–Overlapping Stenosis Model.

among the stenosis configurations. Its minimum pressure reaches approximately 17,292 Pa, which is lower than that of the Bell–Overlapping and Cosine–Overlapping geometries, both of which show a minimum pressure of about 17,306 Pa. This indicates that the geometric shape of the stenosis has a stronger influence on pressure behavior than the stenosis length itself. The double-curved structure characteristic of the Overlapping geometries may contribute to their reduced sensitivity to pressure changes. Similar to the velocity results, variations in stenosis length do not alter the minimum pressure value but do expand the region experiencing low pressure. Furthermore, the predicted minimum pressure range (17.29–17.31 kPa) is consistent with physiological values reported in Goldenberg et al. [22] and Ding et al. [23], indicating that the model remains well aligned with clinically observed hemodynamic conditions. From a clinical perspective, the presence of lower pressure and the widening of the low-pressure region in longer stenosis segments may indicate a broader area of reduced perfusion within the retinal artery. Such conditions can potentially contribute to retinal hypoperfusion and ischemia, which are key pathological mechanisms associated with Branch Retinal Artery Occlusion (BRAO). Reduced perfusion pressure in the retinal circulation can impair oxygen and nutrient delivery to retinal tissues, potentially leading to localized ischemic injury and visual field defects.

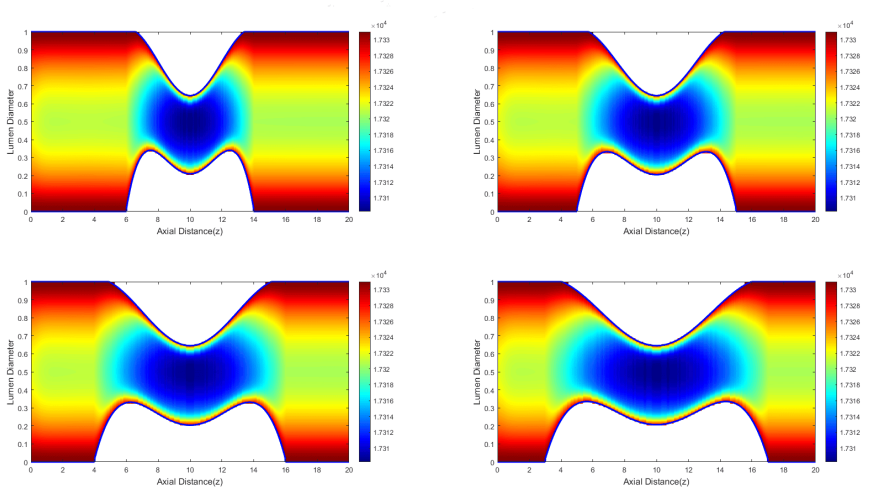

Figure 10. Pressure Distribution Generated by MATLAB for Cosine–Overlapping Geometry.

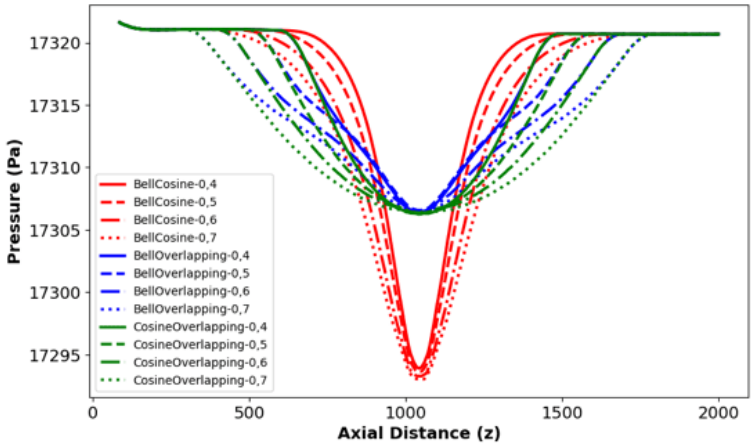

Figure 11. Pressure Profiles Under Stenosis Length Variations for All Geometric Configurations.

Clinical investigations have reported that insufficient retinal perfusion is strongly associated with the development of ischemic retinal damage and progressive visual impairment in BRAO patients. Previous ophthalmologic studies have also emphasized that alterations in retinal blood flow and perfusion pressure play a crucial role in the onset and progression of retinal arterial occlusive diseases, particularly in regions downstream of arterial narrowing where tissue oxygen supply becomes compromised [24, 25]. These findings support the physiological relevance of the present simulation results and suggest that the predicted low-pressure regions may correspond to clinically significant zones of potential retinal ischemia.

A mesh-independence study was performed using element sizes of 0.02 mm, 0.015 mm, and 0.01 mm. The difference in peak velocity between the two finest meshes was less than 1.2%, indicating satisfactory mesh convergence and numerical stability of the solution. Model validation was carried out by comparing the predicted physiological pressure (17.2–17.4 kPa) and velocity range $\left(0.19 - 0.49\ \frac{\mathrm{m}}{\mathrm{s}}\right)$ with experimental and clinical values reported by Goldenberg et al. [22] and Ding et al. [23]. The close agreement between the simulation results and previously reported physiological data confirms the reliability of the numerical model in representing retinal hemodynamic conditions. Furthermore, the use of a finite volume framework implemented in MATLAB, combined with verification through ANSYS FLUENT simulations, provides additional cross-platform confirmation of the

numerical accuracy and robustness of the predicted flow behavior under Branch Retinal Artery Occlusion (BRAO) conditions.

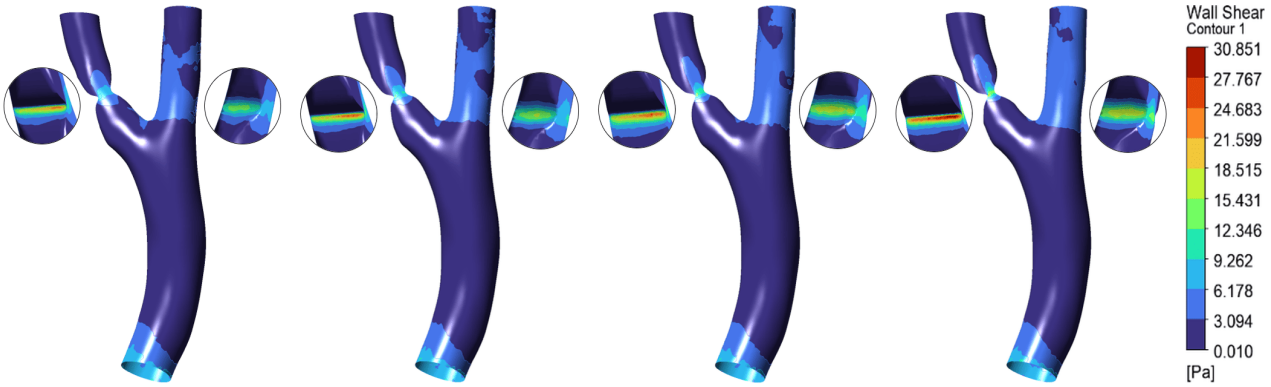

Figure 12. Wall Shear Stress Distribution with Bell–Cosine Geometry.

Figure 12 illustrates the wall shear stress (WSS) distribution in a bifurcated retinal artery with Bell–Cosine stenosis geometry, representing conditions related to Branch Retinal Artery Occlusion (BRAO). The WSS values range from approximately 0.010 Pa to 30.851 Pa. In most parts of the vessel, the WSS remains relatively low, generally below 6 Pa, which is indicated by the dark blue contours and corresponds to regions where the vessel diameter is wider and the flow is more stable. A significant increase in WSS occurs at the stenosis throat, where the vessel narrowing causes the blood flow to accelerate, resulting in higher shear stress values between 21.599 Pa and 30.851 Pa. This indicates that the strongest mechanical forces act on the arterial wall at the narrowest part of the vessel. After the flow passes through the stenosis, the WSS gradually decreases to moderate values between 9.262 Pa and 18.515 Pa due to the expansion of the flow. Further downstream, the WSS returns to lower values as the flow becomes more stable. In the context of BRAO, this pattern suggests that the stenotic region experiences the highest shear stress, which may contribute to endothelial damage and disturbances in retinal blood circulation.

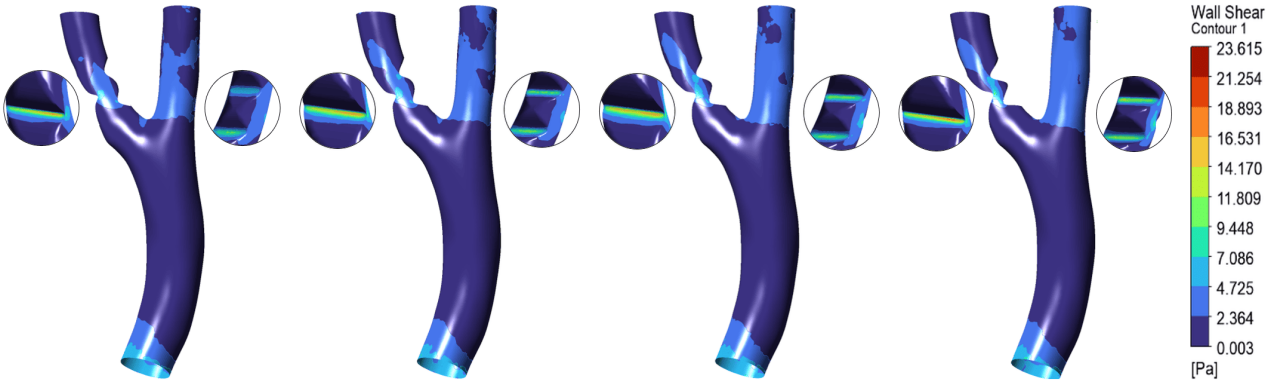

Figure 13. Wall Shear Stress Distribution with Bell–Overlapping Geometry.

Figure 13 shows the wall shear stress (WSS) distribution in a bifurcated retinal artery with Bell–Overlapping stenosis geometry, representing the hemodynamic condition associated with Branch Retinal Artery Occlusion (BRAO). The WSS values range from approximately 0.003 Pa to 23.615 Pa. In most regions of the vessel, the WSS remains relatively low, generally below 4.725 Pa, which is indicated by the dark blue contours and corresponds to wider vessel regions where the blood flow is relatively stable. A noticeable increase in WSS occurs at the stenosis throat, where the narrowing of

the artery accelerates the blood flow and produces higher shear stress values between 16.531 Pa and 23.615 Pa, represented by yellow to red colors. This indicates that the strongest mechanical forces act on the vessel wall at the most constricted region. After passing through the stenosis, the WSS gradually decreases to moderate values of approximately 7.086 Pa to 14.170 Pa as the flow expands and the velocity gradient near the wall becomes smaller. Further downstream, the WSS returns to lower values as the flow stabilizes along the arterial branches. In the context of BRAO, this pattern suggests that the stenotic region experiences the highest shear stress, which may contribute to endothelial stress and disturbances in retinal blood circulation.

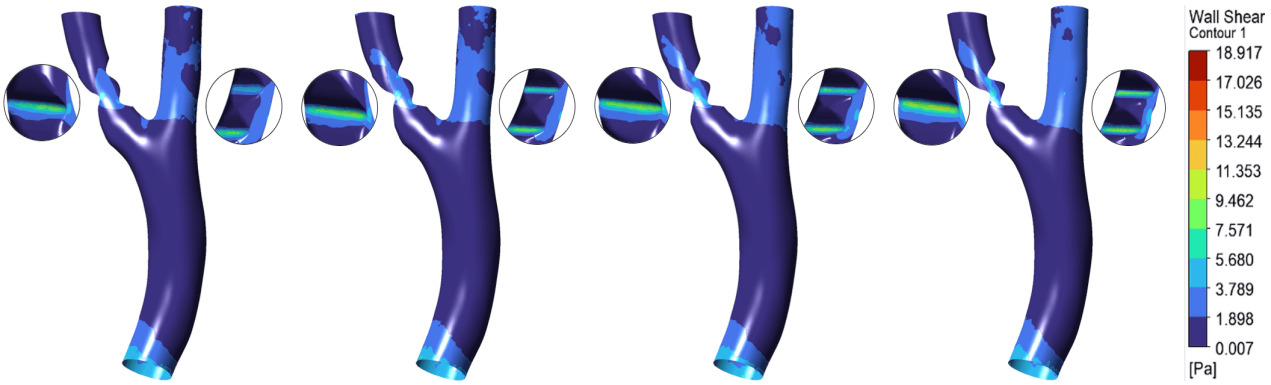

Figure 14. Wall Shear Stress Distribution with Cosine–Overlapping Geometry.

Figure 14 shows the wall shear stress (WSS) distribution in a bifurcated retinal artery with Cosine–Overlapping stenosis geometry, representing hemodynamic conditions associated with Branch Retinal Artery Occlusion (BRAO). The WSS values range from approximately 0.007 Pa to 18.917 Pa. In most regions of the artery, the WSS remains relatively low, generally below 3.789 Pa, which is indicated by the dark blue contours and corresponds to wider vessel areas where the blood flow is relatively stable. A clear increase in WSS occurs at the stenosis throat, where the vessel narrowing accelerates the blood flow and produces higher shear stress values between 13.244 Pa and 18.917 Pa, represented by yellow to red colors. This indicates that the strongest mechanical forces act on the vessel wall at the most constricted part of the artery. After the blood passes through the stenotic region, the WSS gradually decreases to moderate values between 5.680 Pa and 11.353 Pa as the flow expands and the velocity gradient near the wall becomes smaller. Further downstream, the WSS returns to lower values as the flow becomes more stable along the arterial branches. In the context of BRAO, this distribution suggests that the stenosis region experiences the highest shear stress, which may influence endothelial stress and contribute to disturbances in retinal blood circulation.

Based on the three geometries shown in Figures 12 to 14, differences in wall shear stress (WSS) distribution indicate varying levels of hemodynamic risk associated with Branch Retinal Artery Occlusion (BRAO). The Bell–Cosine geometry exhibits the highest WSS values, reaching approximately 30.851 Pa at the stenosis throat, indicating a strong acceleration of blood flow through the narrowed region and producing the largest mechanical stress on the arterial wall. In comparison, the Bell–Overlapping geometry shows a lower peak WSS of about 23.615 Pa, suggesting a moderate level of shear stress concentration in the stenotic region. Meanwhile, the Cosine–Overlapping geometry produces the lowest peak WSS, around 18.917 Pa, indicating a relatively weaker shear stress intensity compared to the other two geometries. Although all three cases demonstrate similar patterns, where WSS increases significantly at the stenosis throat and decreases downstream due to flow expansion, the magnitude of the peak stress differs considerably. In the context of BRAO, higher WSS at the stenotic region can increase endothelial stress and potentially accelerate vascular damage or plaque instability. Therefore, among the three geometries, the Bell–Cosine stenosis appears to present the

highest hemodynamic risk for BRAO, followed by Bell–Overlapping, while Cosine–Overlapping shows the lowest relative risk due to its smaller peak WSS and more moderate shear stress distribution.

5. Conclusion

This study has investigated the effect of varying stenosis lengths in BRAO by simulating how these constrictions influence blood flow behavior. Using stenosis lengths ranging from 40 to 70 μm, the key findings of this research can be summarized as follows:

1. The Bell–Cosine geometry exhibits the highest velocity and the lowest pressure among all stenosis shapes, across every length variation. These conditions may pose potential risks, as elevated velocity and reduced pressure can contribute to more severe flow disturbances.
2. Stenosis length does not significantly affect the maximum velocity or minimum pressure. Instead, variations in length primarily influence the width of the velocity and pressure curves. This indicates that stenosis length affects the distribution of the flow field rather than the peak values of velocity or pressure.
3. The wall shear stress (WSS) distribution is strongly influenced by the stenosis geometry. Among the three models, the Bell–Cosine geometry produces the highest peak WSS, followed by the Bell–Overlapping and Cosine–Overlapping geometries. Higher WSS occurs at the stenosis throat due to flow acceleration in the narrowed region, indicating greater mechanical stress on the vessel wall and a higher potential risk for hemodynamic disturbance in BRAO.

Overall, the simulation results demonstrate that the proposed model is effective for evaluating blood flow velocity and pressure in cases of BRAO.

Supplementary Information

Author Contributions. **Basuki Widodo:** Conceived the study, developed the research framework, supervised the project, and critically revised the manuscript. **Ni Putu Anna Ristia Dewi:** Developed the mathematical model, including derivation of governing equations, nondimensionalization, and theoretical analysis. **Yuni Keputri Muarifadila:** Performed numerical simulations, implemented computational methods, analyzed data, and validated results. **Annisa Dwi Sulistyaningtyas:** Designed stenosis geometries, prepared visualizations, and drafted the manuscript. **Arif Fatahillah:** Provided clinical insights, ensured physiological relevance, and contributed to the interpretation of results. **Tri Rahayuningsih:** Provided clinical insights, ensured physiological relevance, and contributed to the interpretation of results.

Acknowledgements. The authors gratefully acknowledge the support of the Laboratory of Modelling and Simulation (LIMOSIM), Department of Mathematics, Sepuluh Nopember Institute of Technology (ITS), Surabaya, Indonesia.

Funding. This research was supported by the Directorate of Research and Community Service (DRPM ITS), Sepuluh Nopember Institute of Technology, through the Strategic Research Grant (SRG) Scheme Assignment Research Funding Agreement Type C of Sepuluh Nopember Institute of Technology Funds in 2026 Number: 1451/PKS/ ITS/2026 Dated February 10, 2026.

Conflict of interest. The authors declare no conflict of interest.

Data availability. Data used to support the findings of this study are included in the article. The authors used parameter values whose sources are from the literature as shown in Table 1.

References

[1] Biehler R, Scholz RW, Straßer R, Winkelmann B. Didactics of Mathematics as a Scientific Discipline. Dordrecht: Kluwer Academic Publishers; 2002. doi:10.1007/0-306-47204-x.

[2] Versteeg MW H K. An introduction to computational fluid dynamics: The finite volume method (2nd ed.). vol. M. 2nd ed. Harlow, England: Pearson Education; 2007.

[3] Lu Y, Bernabeu MO, Lammer J, Cai CC, Jones ML, Franco CA, et al. Computational fluid dynamics assisted characterization of parafoveal hemodynamics in normal and diabetic eyes using adaptive optics scanning laser ophthalmoscopy. Biomedical Optics Express. 2016 dec;7(12):4958. doi:10.1364/boe.7.004958.

[4] Ong CW, Tan B, Hussain S, Chuangsuwanich T, Braeu FA, Cui F. Evaluation of the effect of hemodynamic factors on

retinal microcirculation by using 3D confocal image-based computational fluid dynamics. Frontiers in Bioengineering and Biotechnology. 2024 nov;12. doi:10.3389/fbioe.2024.1489172.

[5] Bénard-Séguin É, Nahab F, Pendley AM, Rodriguez Duran M, Torres Soto M, Keadey M, et al. Eye stroke protocol in in the emergency department. Journal of Stroke and Cerebrovascular Diseases. 2024;33(9):107895. doi:10.1016/j.jstrokecerebrovasdis.2024.107895.

[6] Genevois O, Paques M, Simonutti M, Sercombe R, Seylaz J, Gaudric A, et al. Microvascular Remodeling after Occlusion-Recanalization of a Branch Retinal Vein in Rats. Investigative Ophthalmology and Visual Science. 2004 feb;45(2):594-600. doi:10.1167/iovs.03-0764.

[7] Mason JO, Shah AA, Vail RS, Nixon PA, Ready EL, Kimble JA. Branch Retinal Artery Occlusion: Visual Prognosis. American Journal of Ophthalmology. 2008;146(3):455-7. doi:10.1016/j.ajo.2008.05.009.

[8] Toolan KJ, Minaker S, Civantos J. Branch retinal artery occlusion (BRAO) after macroaneurysm. American Journal of Ophthalmology Case Reports. 2024;36:102108. doi:10.1016/j.ajoc.2024.102108.

[9] Fatahillah A, Widodo B, Roslan R. The Modeling and Numerical Solution of Branch Retinal Artery Occlusion. Malaysian Journal of Mathematical Sciences. 2025;19(1):1-16. doi:10.47836/mjms.19.1.01.

[10] Kumar S, Kumar S. Blood Flow with Heat Transfer through Different Geometries of Stenotic Arteries. Trends in Sciences. 2023;20(11):6965. doi:10.48048/tis.2023.6965.

[11] Fatahillah A, Widodo B, Roslan R. Mathematical Modeling and Numerical Simulation of Central Retinal Artery Occlusion (CRAO) with Asymmetric Stenosis. Statistics, Optimization and Information Computing. 2025;13(5):2079-104. doi:10.19139/soic-2310-5070-2381.

[12] Aruchamy P, Mahagaonkar P, Ganesan G, Dhandapani PB, Yahya NI. Identifying the Fetal Heart Rate and Gender with Intuitionistic Fuzzy Total Edge Magic Labelling. Jambura Journal of Biomathematics (JJBM). 2025;6(2):159-65. doi:10.37905/jjbm.v6i2.30951.

[13] Das K, Kumar GR, Ramesh K, Biswas MHA. A Qualitative Analysis of Leukemia Fractional Order SICW Model. Jambura Journal of Biomathematics (JJBM). 2024;5(1):46-53. doi:10.37905/jjbm.v5i1.24961.

[14] Chung TJ. Computational Fluid Dynamics. Cambridge University Press; 2002. doi:10.1017/CBO9780511606205.

[15] Guidoboni G, Harris A, Carichino L, Arieli Y, Siesky BA. Effect of intraocular pressure on the hemodynamics of the central retinal artery: A mathematical model. Mathematical Biosciences and Engineering. 2014;11(3):523-46. doi:10.3934/mbe.2014.11.523.

[16] Wu LT, Wang JL, Wang YL. Ophthalmic artery morphological and hemodynamic features in acute coronary syndrome. Investigative Ophthalmology and Visual Science. 2021;62(14):7. doi:10.1167/iovs.62.14.7.

[17] Hua Zhou Z, Ru Cheng X, Xin Guan J, Zhao L, ling Wang Y, lin Wang J. A Nomogram Based on Ocular Hemodynamics for Predicting Ischemic Stroke. American Journal of Ophthalmology. 2025;274:91-100. doi:10.1016/j.ajo.2025.02.034.

[18] Kim HM, Woo SJ. Clinical characteristics of recurrent non-arteritic retinal artery occlusion. BMJ Open Ophthalmology. 2024;9(1):e001636. doi:10.1136/bmjophth-2024-001636.

[19] Ismail A, Chen HC, Faye I, Tang TB. Longitudinal effects of common carotid artery stenosis on ocular hemodynamics assessed using laser speckle flowgraphy in a rabbit model. Scientific Reports. 2020;10(1):15829. doi:10.1038/s41598-020-72556-9.

[20] Liu WL, Wu LT, Wang JL, Sun J, Cheng XR, Zhou ZH, et al. Effect of PCI on ophthalmic artery hemodynamics in patients with acute coronary syndrome. Frontiers in Medicine. 2024;11:1367900. doi:10.3389/fmed.2024.1367900.

[21] De Salvo G, Oshallah M, Sepetis AE, Borbara R, Oliverio GW, Meduri A, et al. Inner Retinal Thinning Comparison between Branch Retinal Artery Occlusion and Primary Open-Angle Glaucoma. Diagnostics. 2023;13(22):3428. doi:10.3390/diagnostics13223428.

[22] Goldenberg D, Shahar J, Loewenstein A, Goldstein M. Diameters of retinal blood vessels in a healthy cohort as measured by spectral domain optical coherence tomography. Retina. 2013;33(9):1888-94. doi:10.1097/IAE.0b013e31829477f2.

[23] Ding Y, Jiang Z, Jiang J, Yang G, Li Y, Tao L. Computational assessment of blood lipid influence on hemodynamics in human retinal vessels. Scientific Reports. 2025;15(1):16542. doi:10.1038/s41598-025-98767-6.

[24] Hayreh SS. Acute retinal arterial occlusive disorders. Progress in Retinal and Eye Research. 2011;30(5):359-94. doi:10.1016/j.preteyeres.2011.05.001.

[25] Yu DY, Cringle SJ, Balaratnasingam C, Morgan WH, Yu PK, Su EN. Retinal ganglion cells: Energetics, compartmentation, axonal transport, cytoskeletons and vulnerability. Progress in Retinal and Eye Research. 2013;36:217-46. doi:10.1016/j.preteyeres.2013.07.001.